Atmospheric Pressure Laser-Induced Acoustic Desorption Chemical Ionization Fourier Transform Ion Cyclotron Resonance Mass Spectrometry for the Analysis of Complex Mixtures

ARTICLE *in* ANALYTICAL CHEMISTRY · FEBRUARY 2011

Impact Factor: 5.64 · DOI: 10.1021/ac102543s · Source: PubMed

5 AUTHORS, INCLUDING:

Amy M. Mckenna
Florida State University
54 PUBLICATIONS **980** CITATIONS

analytical chemistry

ARTICLE

pubs.acs.org/ac

Atmospheric Pressure Laser-Induced Acoustic Desorption Chemical Ionization Fourier Transform Ion Cyclotron Resonance Mass Spectrometry for the Analysis of Complex Mixtures

Leonard Nyadong,[†] Amy M. McKenna,[†] Christopher L. Hendrickson,[†,‡] Ryan P. Rodgers,[*,†,‡] and Alan G. Marshall[*,†,‡]

[†]Department of Chemistry and Biochemistry, Florida State University, 95 Chieftain Way, Tallahassee, Florida 32303, United States

[‡]National High Magnetic Field Laboratory, Florida State University, 1800 East Paul Dirac Drive, Tallahassee Florida 32310-4005, United States

Supporting Information

ABSTRACT: We present a novel nonresonant laser-based matrix-free atmospheric pressure ionization technique, atmospheric pressure laser-induced acoustic desorption chemical ionization (AP/LIAD-CI). The technique decouples analyte desorption from subsequent ionization by reagent ions generated from a corona discharge initiated in ambient air or in the presence of vaporized toluene as a CI dopant at room temperature. Analyte desorption is initiated by a shock wave induced in a titanium foil coated with electrosprayed sample, irradiated from the rear side by high-energy laser pulses. The technique enables facile and independent optimization of the analyte desorption, ionization, and sampling events, for coupling to any mass analyzer with an AP interface. Moreover, the generated analyte ions are efficiently thermalized by collisions with atmospheric gases, thereby reducing fragmentation. We have coupled AP/LIAD-CI to ultrahigh-resolution FT-ICR MS to generate predominantly $[M + H]^+$ or $M^{+\bullet}$ ions to resolve and identify thousands of elemental compositions from organic mixtures as complex as petroleum crude oil distillates. Finally, we have optimized the AP/LIAD CI process and investigated ionization mechanisms by systematic variation of placement of the sample, placement of the corona discharge needle, discharge current, gas flow rate, and inclusion of toluene as a dopant.

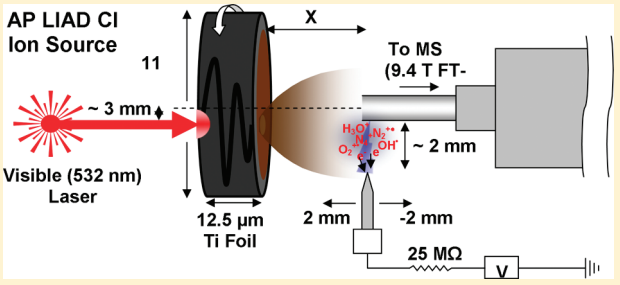

The introduction of soft ionization techniques, particularly electrospray ionization (ESI) by Fenn[1] and co-workers and matrix-assisted laser desorption ionization (MALDI) by Tanaka et al.[2] and Karas and Hillenkamp[3,4] have revolutionized the analysis of thermally labile nonvolatile molecules. Those techniques are however limited to the analysis of molecules of medium to high polarity, for which ionization occurs mainly by protonation/deprotonation and/or ion (cation or anion) attachment. The laser desorption/ionization efficiency of MALDI is particularly limited by the requirement of the matrix to be miscible and to form cocrystals with the analyte. Moreover, interference from matrix cluster ion signals in the low mass range (m/z < 500) limits its capability for the analysis of small molecules.[5,6]

Laser-induced acoustic desorption (LIAD)[7−16] is a nonresonant matrix-free laser-based technique that has been implemented mainly in vacuum for the analysis of thermally labile compounds. This technique was first coupled to mass spectrometry in the mid-1980s by Lindner and Seydel.[17] Unlike MALDI and other laser desorption techniques, the sample is not directly exposed to intense laser light, making it especially powerful for the analysis of light-sensitive small molecules. In LIAD, a sample deposited onto a thin metal foil is irradiated from the back side with a series of high-energy laser pulses. The resulting high amplitude acoustic waves that propagate through the foil cause the desorption of analyte species with exceptionally low gas-phase internal energy.[15] Lindner and Seydel proposed that most of the mechanical energy provided by the acoustic wave was coupled into the desorption event, with inadequate energy for ionization, resulting predominantly in gas phase neutral analytes except when precharged in solution prior to deposition.[17] LIAD essentially decouples analyte desorption from subsequent ionization, enabling coupling to a broad range of ionization techniques.[12,14,16,18] Because of its low thermal conductivity and expansion coefficient, Ti foil has most commonly been used as a LIAD target to minimize the amount of thermal energy that reaches the analyte.[14]

Chemical ionization (CI) has been the primary ionization method coupled with LIAD.[7,8,10,11,13,14] In CI, electrons generated from a corona discharge, ^{63}Ni (as in APCI), or an electron gun (such as in vacuum CI) interact with reagent gases to initiate a series of reactions that generate reagent ions. Vaporized neutral analytes are then ionized by chemical reaction with those reagent ions. Compared to other ionization techniques that have been coupled to LIAD in vacuum (e.g., electron ionization, EI[12] and

Received: September 26, 2010
Accepted: January 11, 2011
Published: February 09, 2011

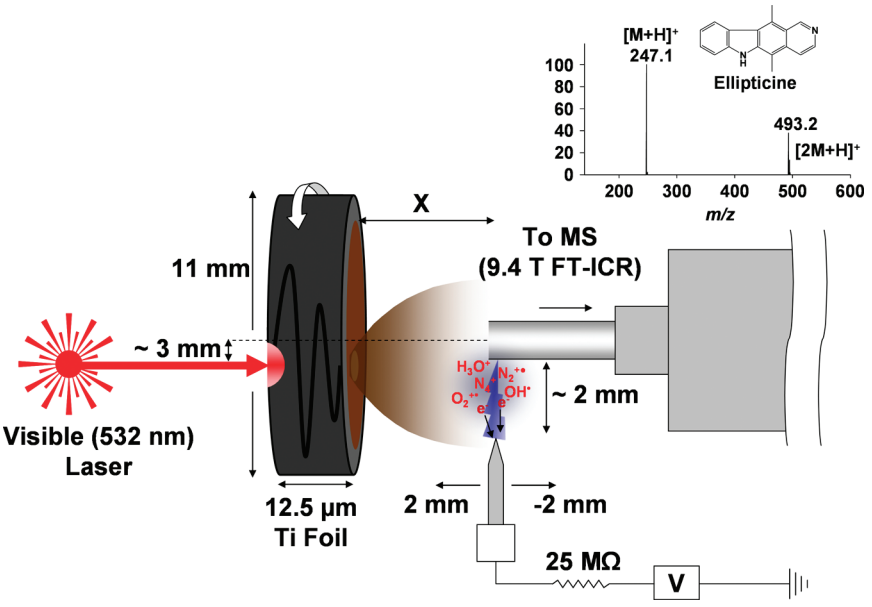

Figure 1. Schematic diagram of an atmospheric pressure laser-induced acoustic desorption chemical ionization (AP/LIAD-CI) source coupled to a 9.4 T Fourier transform ion cyclotron resonance mass spectrometer. The inset show the mass spectra obtained for a petroleum model compound (ellipticine) following LIAD with the corona discharge on.

photon ionization, PI[16]), the reagent ion cloud in CI appears to provide the most efficient ionization. Moreover, CI provides a wide range of ionization channels in addition to those provided by ESI and MALDI, including: charge exchange, hydride abstraction, electron capture, etc.[19−22] CI is therefore very attractive for analysis of complex mixtures containing compounds with a broad range of polarity and functionality (such as petroleum crude oil), because ionization conditions can be tuned to favor particular chemical components. Finally, CI can be tailored to generate intact analyte ions (e.g., for complex mixtures) or induce fragmentation to provide structural information.

The coupling of LIAD to CI has typically been performed by trapping and accumulating reagent ions prior to LIAD,[10−14] to increase the chance of collision/reaction with analytes. Thus, LIAD has mainly been performed in vacuum, in which reagent ions of interest are first trapped in an ICR cell,[7,11,13−15] or an ion trap[10] for efficient ionization of the analyte plume as it diffuses through the reagent ion cloud. Operation in vacuum however significantly limits the throughput (and thus impact) of the technique, requiring special instrumentation, limiting its appeal to the mass spectrometry community.

The implementation of LIAD at atmospheric pressure (AP) is especially attractive because it allows facile and independent optimization of the analyte desorption, ionization and sampling events.[7,11,13,14] It also allows the technique to be coupled to any mass analyzer with an AP interface.

Shiea et al. recently coupled LIAD to ESI for analysis of peptides/protein and analytes separated by thin layer chromatograph (TLC).[18,23] However, that technique suffers from the inherent limitations of ESI. Here, we introduce the implementation of LIAD at AP, with analyte ionization by CI, based on reagent ions generated from a corona discharge in ambient air and in the presence of vaporized toluene as dopant at room temperature, coupled to an FT-ICR mass spectrometer. We thereby combine the many ionization channels provided by CI with the high mass resolution/accuracy of FT-ICR MS to provide a state of the art analysis platform for the reliable determination of the composition of complex mixtures. We present initial results on the optimization and characterization of the AP/LIAD-CI ion source, applied to analysis of petroleum model compounds (polar and nonpolar), as well as a heavy vacuum gas oil (HVGO) distillate fraction from Athabasca bitumen.

EXPERIMENTAL METHODS

Samples and Reagents. All reagents and samples were used without additional purification. HPLC grade toluene (99.9% Sigma Aldrich, St. Louis, MO, USA) was evaluated as a dopant for CI. The performance of the ion source was characterized by use of the following petroleum model compounds: ellipticine, perylene, diphenylbenzoquinoline, benzo(ghi)perylene, coronene, rubrene, 9-phenylanthracene, benzo[*c*]benzofuran, benzo-[*c*]benzothiophene, and the hormone, estradiol, purchased from Sigma Aldrich (St. Louis, MO, USA). Tetradecylpyrene, tetraphenylthiophene and MG 613, generously provided by Prof. Murray Gray of the University of Alberta, were also evaluated.[24] Industrial grade N_2 (99.998% Airgas South, Tallahassee, FL) was used to vaporize and transport the dopant into the ion source chamber. The ion source performance was also evaluated at various flow rates of breathing grade air (Airgas South, Tallahassee, FL) introduced into the source chamber following initiation of a corona discharge in ambient air. A crude oil distillate 400−425 °C was obtained by fractionation of an Athabasca bitumen HVGO.[25−27]

AP/LIAD-CI Ion Source. Figure 1 is a schematic diagram of the experimental setup. The AP/LIAD-CI source was interfaced to a custom-built 9.4 T FT-ICR mass spectrometer[28,29] by means of a reconfigured APCI source chamber (Thermo Finnigan, San Jose, CA, USA, not shown in Figure 1) as follows. The sheath gas/sample introduction port was adapted to hold a corona discharge needle made from a sharpened tungsten electrode (Welding Supply, Elk Grove Village, IL, USA). A discharge was initiated between the tungsten electrode regulated from 2.5 to 4.5 kV by a high-voltage power supply (SRS PS350, Sunnyvale, CA, USA) and

the MS inlet capillary held at 70 V (discharge current, 9−12 μA, unless stated otherwise). The needle was oriented orthogonal to the MS capillary inlet, 1−2 mm away from the outer surface (Figure 1). The needle could be translated along the length of the capillary, about the inlet to vary the concentration of reagent ions interacting with the neutral plume within the sample-MS interface. The aperture in the source chamber that normally holds the needle was used to mount a LIAD probe that was inserted and secured in its associated screw fitting. The probe consisted of a 13 cm hollow Teflon cylinder (11 mm i.d., 18.4 mm o.d., Upchurch Scientific, Oak Harbor, WA, USA) fitted with a hollow stainless steel (ss) disk on one end. The ss disk (1.3 mm thickness, 11 mm i.d., 18.4 mm o.d.) was used to sandwich a sample-containing piece of Ti foil (12.7 μm thickness) onto the Teflon cylinder. The assembly was held in place by four set screws mounted on the ss disk and threaded into the Teflon body. The probe could be translated back and forth to adjust the sample-to-MS distance. It could also be rotated about its longitudinal axis to expose different positions on the back side of the Ti foil (Alfa Aesar, Ward Hill, MA, USA) to the laser beam during LIAD. The port that normally holds the voltage connections to the heater was adapted to hold a male-to-male swagelok fitting (Swagelok Company, Solon, OH, USA) attached to 1/8″ Teflon tubing to introduce gases and/or dopant into the ion source chamber. Vaporized dopant (toluene) was generated by bubbling N_2 (400 mL/min) at room temperature through the solvent contained in a glass vial. A second Teflon tubing connection between the solvent-containing vial and the ion source chamber was used to transport the vaporized dopant into the ion source.

Sample Preparation for AP/LIAD-CI. Samples for ion source optimization experiments were prepared by use of an ellipticine standard (1.25 mM in 75:25 MeOH/toluene) electrosprayed onto a Ti foil. For each experiment, 20 μL of the sample solution was deposited on the foil at a flow rate of 2 μL/min and a sprayer-to-target distance of ∼10 mm to deposit analyte over an ∼11.5 mm diameter area. Ion source characterization under various CI conditions was performed for various petroleum model compounds pipet-spotted (2 μL, 0.25 mM in toluene) onto a Ti foil and analyzed following solvent evaporation. An equimolar mixture of benzo(ghi)perylene, diphenylbenzoquinoline, coronene, tetradecylpyrene and ellipticine was prepared by mixing 100 μL, 1 mM of each compound. Two microliters of the mixture was spotted onto a Ti foil and analyzed following solvent evaporation. The HVGO distillate sample was prepared similarly with 4 μL, 1 mg/mL of sample in toluene. Samples spotted from a solution in 100% toluene result in minimal spread on the foil surface to give a better focused sample area compared to spotting from solvent mixtures containing various proportion of MeOH.

For AP/LIAD-CI experiments, an analyte-coated Ti foil was mounted on the LIAD probe and inserted into the source chamber, and the sample-to-MS distance adjusted to ∼6 mm unless stated otherwise. The rear side of the foil was then irradiated with a pulsed Q-switched Nd:YAG laser beam (Surelite I, Continuum, Santa Clara, CA, USA) through ambient air. The laser was operated at 532 nm, pulsed at 10 Hz, with pulse energy ranging from 53−105 mJ and pulse duration of ∼5 ns creating a 4.4 mm diameter spot on the rear side of the foil, corresponding to a power density of (0.7−1.4) × 10^8 W/cm^2. Following laser ablation, the vaporized analyte plume of neutrals generated on the opposite side of the foil was ionized by CI through collisions with reagent ions generated by a corona discharge initiated either in ambient air or in the presence of vaporized toluene as dopant.

9.4 T FT-ICR MS and Data Analysis. The mass spectrometer is a custom-built FT-ICR instrument.[30,31] All experiments were performed with positive ions unless stated otherwise. AP/LIAD-CI generated ions traverse a heated metal capillary into a first octopole, in which the ions are accumulated for a very short period (70 ms). The ions are then transferred through a quadrupole to a second octopole, in which they are further accumulated for a total of 15 injections from the first octopole. The laser pulse rate was synchronized with the duration of the accumulation and transfer of ions from the first octopole. Helium gas was introduced into the second octopole to collisionally cool the ions prior to transfer through a set of three rf-only octopole guides (127 cm total length) into an open cylindrical ion trap (10 cm i.d., 30 cm long).[32] The ions were cyclotron-excited by broadband frequency sweep (chirp) excitation and were subsequently detected as the differential current induced between two opposed electrodes of the ICR cell. Each AP/LIAD-CI MS experiment was performed by averaging 1−10 time-domain MS acquisitions, corresponding to 15−150 laser shots during which the LIAD probe was manually rotated at ∼7 rpm about its longitudinal axis. Each of the acquisitions was Hanning-apodized and zero-filled prior to fast Fourier transform and magnitude calculation.[33] The experimental event sequence was controlled by a modular ICR data acquisition system.[30] Infrared multiphoton dissociation (IRMPD) was performed in the ICR cell to decluster multimers if necessary, by irradiating the ions with a 28 W continuous CO_2 laser (λ = 10 μM, Synrad model J48−2, Mulkilteo, WA, USA) beam for 100 ms.[34,35]

The AP/LIAD-CI FT-ICR mass spectrum of the petroleum distillate sample was internally calibrated with respect to a highly abundant homologous alkylation series with a recently reported novel calibration technique.[35] Singly charged ions with relative abundance greater than six standard deviations of the baseline root-mean-square (rms) noise were exported to a spreadsheet, after conversion to the Kendrick mass scale[36] for easier identification of homologous series (i.e., species with the same $N_nO_oS_s$ content, differing only by degree of alkylation) and peak assignments were performed by Kendrick mass defect analysis.[37] For each elemental composition, $C_cH_hN_nO_oS_s$, the heteroatom class, type (double bond equivalents, DBE, defined as the number of rings plus double bonds to carbon),[38] and carbon number, c, were tabulated for generation of heteroatom class relative abundance distributions and graphical DBE versus carbon number images.

RESULTS AND DISCUSSION

LIAD Produces Gas-Phase Neutral Analytes; Corona Discharge Generates Positive and Negative Ions. Initial proof-of-concept and ion source characterization experiments were performed with ellipticine, a petroleum model compound electrosprayed onto a Ti foil. A corona discharge initiated in ambient air generates reactive species for chemical ionization of vaporized analytes (Supporting Information Scheme S-1, chemical reactions i−vii). Laser-induced acoustic desorption[11,13,14] of neutrals from the Ti foil occurred at a threshold energy density of 0.7 × 10^8 W/cm^2, as readily verified by visual inspection of the foil. However, no ion signal was observed at that energy density and beyond if the corona discharge was off. With the corona discharge on, peaks corresponding to protonated ellipticine monomer, m/z 247.1, and dimer, m/z 493.2, were readily observed (Figure 1). LIAD generates predominantly gas-phase

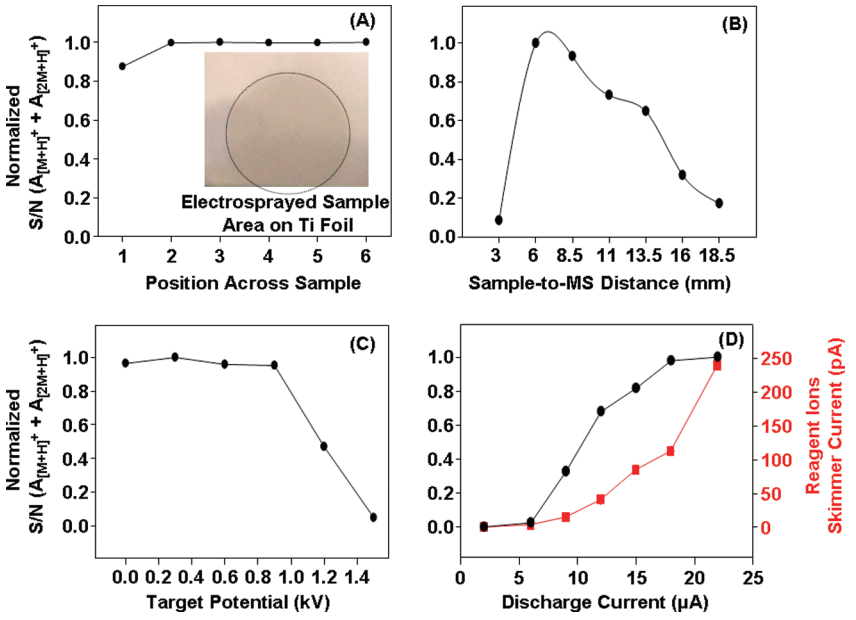

Figure 2. (●) AP/LIAD-CI MS signal for ellipticine standards (20 μL, 1.25 mM) electrosprayed onto Ti foil targets as a function of: (A) location of laser ablation on the rear side of the foil, (B) sample-to-MS orifice distance (X), (C) potential on the Ti foil target, and (D) corona discharge current. The red trace in Figure 2D (■) is the current measured on the skimmer as a function of ambient air corona discharge current in the absence of LIAD.

neutral analytes, as expected, requiring a secondary means for ionization. For experiments performed in the presence of IRMPD, the peak corresponding to the dimer was readily dissociated resulting predominantly in the protonated ellipticine monomer (Supporting Information Figure S1, top). The dissociation of the dimer simplifies the mass spectrum and increases signal-to-noise ratio. For a negative corona discharge, negative ions corresponding to deprotonated ellipticine monomer, m/z 245.1, and dimer, m/z 491.1, were also detected (Supporting Information Figure S1, bottom). All experiments reported from here on are for positive ions.

The analyte signal magnitude showed very little dependence on the alignment of the laser beam with the MS inlet capillary. The laser beam could thus be offset by ~3 mm from the axis of the inlet capillary to expose different positions on the back side of the foil for laser ablation following translation of the probe along its longitudinal axis (Figure 1). The increased analysis period enables more MS acquisitions, which may be averaged to obtain better signal-to-noise ratio and mass accuracy.

Optimizing AP/LIAD-CI FT-ICR MS Signal: Sample-to-MS Inlet Distance. Electrospray sample deposition resulted in a relatively uniform analyte distribution as determined by visual inspection of the sample spot (Figure 2). AP/LIAD-CI of distinct spots across the rear side of the foil resulted in 5% relative standard deviation for the MS signal (Figure 2A), verifying the relatively homogeneous distribution of analyte over the electrosprayed spot and validating the utility of this sample preparation protocol for ion source optimization experiments.

The sample-to-MS distance (X in Figure 1) was the most critical in determining MS signal magnitude. Below the optimum sample-to-MS distance (~6 mm, see Figure 2B), the period for interaction between the expanding analyte plume and the reagent ions decreases, resulting in lower signal magnitude. For sample-to-MS distance greater than 6 mm, the dispersing analyte stream becomes more dilute as it reaches the MS capillary inlet, also resulting in reduced signal magnitude.

As the target potential (i.e., the voltage applied to the sample-containing Ti foil) increases from 0 kV to ~1 kV, the signal magnitude stays very much the same (Figure 2C), and decreases sharply at higher voltage (>1 kV). The relative independence of the signal magnitude with respect to the target potential at lower voltage (<1 kV) indicates that analytes are vaporized predominantly as neutrals by LIAD as previously reported, and require an independent process for ionization.[17] Above 1 kV, the MS capillary starts discharging with the target and the path of the current breakdown interferes with ion transmission into the MS capillary inlet, thereby decreasing the signal (Figure 2C).

The analyte signal magnitude also depends strongly on the corona discharge current, increasing with increasing discharge current up to ~22 μA (Figure 2D, ●). The higher reagent ion population (available for ionization) for higher discharge current is verified by the higher ion current measured on the skimmer (i.e., in the absence of LIAD, Figure 2D, ■). Protonated analytes typically predominate at low discharge current (e.g., 9 μA (Supporting Information Figure S2, top)). At higher discharge current (e.g., 36 μA (Figure S2, middle)), oxidation products begin to appear and increase dramatically at even higher current (e.g., 228 μA (Figure S2, bottom)), presumably due to the higher population of nitric oxide cations (NO^+, a strong oxidant commonly observed in AP discharge-type ion sources)[39] at higher discharge current. All subsequent experiments were therefore performed at relatively low current (9−12 μA) unless stated otherwise. The signal magnitude also increased with increased surface concentration of the analyte up to ~30 pmol/mm^2, thereby defining the dynamic range for the experiment (Supporting Information Figure S3). Above that range, the signal no longer increases, presumably due to saturation of the ion capacity of the cell. The detection limit ($S/N \geq 3$) for ellipticine was 20 fmol, calculated based on experiments for a single MS acquisition.

Optimizing AP/LIAD-CI FT-ICR MS Signal: Corona Discharge Needle Placement. As shown in Figure 1, the corona discharge needle can be translated along and perpendicular to the

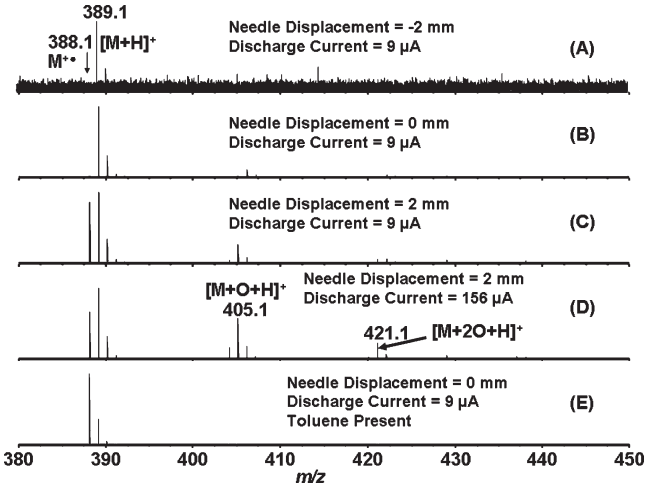

Figure 3. AP/LIAD-CI FT-ICR mass spectra of tetraphenylthiophene for various displacements of the corona discharge needle, along the length of the MS inlet capillary with respect to the inlet position. The distance from the tip of the corona discharge needle to the outer circumference of the inlet capillary was ~2 mm and the discharge current was set at 9 μA (A−C; E) or 156 μA (D). (E) shows the AP/LIAD-CI FT-ICR mass spectrum of tetraphenylthiophene with the needle held at the 0 mm position for corona discharge initiated in the presence of vaporized toluene (dopant).

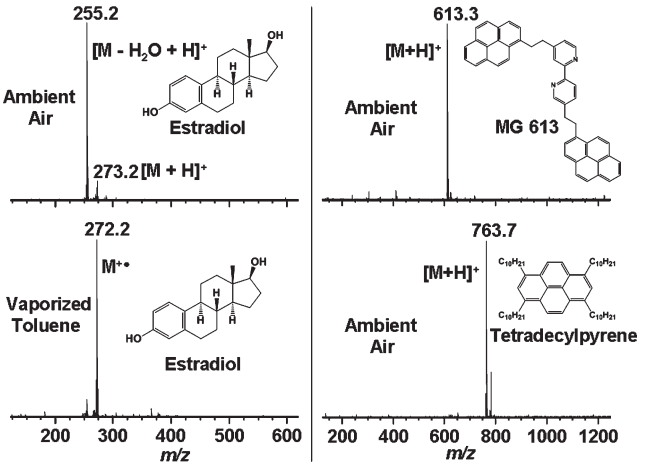

Figure 4. AP/LIAD-CI FT-ICR mass spectra of estradiol from a corona discharge initiated in ambient air and in the presence of vaporized toluene; and MG 613 and tetradecylpyrene in ambient air. The mass spectrum for tetradecylpyrene shows a minor peak at *m/z* 780.7, corresponding to the ammonium adduct of the analyte originating from reaction with ammonium, generated in the corona discharge from traces of ammonia in the laboratory air.

MS capillary. The effect of the longitudinal position of the corona needle (i.e., along the MS capillary, about the inlet, see Figure 1) on ICR signal magnitude and distribution of observed analyte species was evaluated for tetraphenylthiophene, another petroleum model compound. At −2 mm with respect to MS capillary inlet, protonated analytes are the dominant positive ions (Figure 3A). However, moving the needle farther away from the MS capillary inlet increased the yield of all ions and produced additional molecular ions and oxidation products (Figures 3B, C). The signal magnitude of all observed analyte species also increased as the needle was transitioned from right to left because of more complete overlap between the reagent ions and analyte neutrals. Formation of radical molecular ions presumably results from charge exchange with oxygen radical cations (Supporting Information Scheme S1, reactions viii and ix), that also compete with the formation of oxidation products for the needle at the 2 mm position. At much higher discharge current (156 μA), the formation of oxidation products increases relative to molecular ions (Figure 3D), presumably because of the higher population of highly reactive NO^+ at higher discharge current.[39] In the presence of toluene dopant, the molecular ion was predominant, providing a simplified spectrum by avoiding the formation of oxidation products (Figure 3E). The mass spectral peak distribution was independent of the position of the needle and/or magnitude of the discharge current under this condition. The formation of molecular ions in that case is ascribed to charge exchange reactions with toluene radical cations as shown in eq 2.

$$S + e^- \rightarrow S^{+\bullet} + 2e^- \quad (1)$$

$$S^{+\bullet} + M \rightarrow M^{+\bullet} + S \; [IE(M) < 8.8eV,^{40} \; S = \text{toluene}, M = \text{analyte}] \quad (2)$$

Optimizing AP/LIAD-CI FT-ICR MS signal: gas flow rate. Supporting Information Figure S4 shows the effect of introducing breathing grade air at three different flow rates during AP/LIAD-CI FT-ICR MS analysis of coronene. Protonated coronene monomer (*m/z* 301.1), dimer (*m/z* 601.1), and trimer (*m/z* 901.1) were the predominant species at a gas flow rate of 5.8 L/min (Figure 4, top). The abundance of multimer species decreased at higher gas flow rate (9.0 L/min, Figure 4, middle); the base peak at *m/z* 298.1 corresponds to loss of hydrogen from the molecular ion. At the highest gas flow rate (14.4 L/min, Figure 4, bottom), the signal corresponding to the dehydrogenated molecular ion becomes the major peak in the spectrum. The analyte signal magnitude decreases with increased gas flow rate. The lower abundance of multimers at higher gas flow rate is probably due to dispersion of the analyte neutral plume by the gas flow following LIAD to give a more dilute analyte concentration at the MS inlet, reducing the likelihood for multimer formation. The loss of hydrogen from $M^{+\bullet}$ occurs by in-source collision-induced dissociation (CID), in the capillary skimmer region as a result of the relatively high tube lens voltage used in these experiments (350 V). In-source CID was verified by performing similar analysis at increasing tube lens voltage (50−350 V). $M^{+\bullet}$ and $[M + H]^+$ were detected for tube lens voltages of 50−150 V, but no $[M - nH]^{+\bullet}$ species (Supporting Information Figure S5). In the 50−100 V range, the abundance of $[M + H]^+$ increases whereas that of $M^{+\bullet}$ decreases, suggesting a self-protonation mechanism for the generation of $[M + H]^+$ by collision of $M^{+\bullet}$ with M. That reaction is evidently favored if a high population of vaporized analyte is entrained into the MS inlet, for example, at a gas flow rate below 9 L/min introduced into the source chamber. At tube lens voltage above 150 V, up to 3 hydrogen molecules are lost ($[M - 2H]^{+\bullet}$ *m/z* 298.1, $[M - 4H]^{+\bullet}$ *m/z* 296.1 and $[M - 6H]^{+\bullet}$ *m/z* 294.1) from the molecular ion. The abundance of those fragments increases with tube lens voltage up to 350 V except for $[M - 2H]^{+\bullet}$, which decreases above 300 V, suggesting it as the precursor for $[M - 4H]^{+\bullet}$ and $[M - 6H]^{+\bullet}$. Increasing the tube lens voltage increases the kinetic energy of the ions toward the skimmer resulting in more energetic collisions with gaseous molecules in that region resulting in CID. Thus, a tube lens voltage of 50 V was used for all subsequent experiments.

Effect of Toluene Dopant. Figure 4 (left) shows AP/LIAD-CI FT-ICR mass spectra of estradiol for reagent ions generated by a corona discharge in ambient air (top) and in the presence of toluene dopant (bottom). For ambient air, the base peak at m/z 255.2 corresponds to the loss of H_2O from the protonated molecule, $[M + H]^+$. In contrast, in the presence of toluene dopant, the base peak shifts to m/z 272.2, corresponding to the intact molecular radical cation. The generation of intact analyte ions in this case occurs by charge exchange with cation radicals of the dopant, and their nearly equal ionization energy accounts for the lack of fragmentation. The generation of analyte fragment ions as the predominant species from ambient air discharge arises from the large proton affinity difference between the reagent species (water clusters) and the analyte. Similar analysis of various petroleum model compounds containing branched chain functionalities, under similar experimental conditions, gives predominantly intact protonated analytes (Figure 4, right). The generation of intact analytes is particularly important for the analysis of complex mixtures such as petroleum, to enable unambiguous peak assignment. In summary, most of the internal energy gained by the analyte during AP/LIAD-CI is incorporated during the ionization event as in vacuum/LIAD-CI.[11] AP/LIAD-CI is thus a "soft" desorption/ionization technique (at least for the petroleum model compounds investigated here) like electrospray ionization or matrix-assisted laser desorption/ionization. AP/LIAD-CI is also versatile: it can be tuned to generate intact analyte ions and/or induce fragmentation based on the choice of reagent ions.[11]

Polycyclic Aromatics. Supporting Information Table S1 lists the relative abundances of $[M + H]^+$ and $M^{+\bullet}$ ions following AP/LIAD-CI in ambient air or in the presence of toluene dopant, for various individually ionized petroleum model compounds spanning a wide range of polarity. For ambient air, compounds of medium to low polarity yielded both $[M+H]^+$ and $M^{+\bullet}$ species, with $[M + H]^+$ favored for the polar nitrogen-containing compounds. The $[M + H]^+$ and $M^{+\bullet}$ relative abundances were consistent with the magnitude of the differences between the proton affinities and/or ionization energies of analyte and reagent ions. In the presence of toluene dopant, $M^{+\bullet}$ ions were typically the only ionic species for compounds of medium to low polarity, whereas $[M + H]^+$ ions were observed for the polar nitrogen-containing analytes.

Figure 5 affords a comparison of the signal-to-noise ratio (S/N) for each of the analytes for both ambient air and toluene dopant conditions. Except for rubrene and diphenylbenzoquinoline, S/N was more than an order of magnitude higher for compounds of medium to low polarity in the presence of toluene dopant presumably due to their preferential ionization by charge exchange, because the large population of reactive dopant species generated in the discharge increases the probability of collision/ionization. Polar nitrogen-containing analytes that preferentially ionize by proton transfer under both conditions show higher S/N in the ambient air discharge than with toluene dopant due to the large excess of protonated water clusters generated under those conditions.

Organic Mixtures. For ambient air discharge of a mixture containing ellipticine, diphenylbenzoquinoline, coronene, benzo(ghi)perylene, and tetradecylpyrene, protonated ellipticine and diphenylbenzoquinoline were the predominant species in the mass spectrum (Figure 6, top), presumably because of their relatively high proton affinity, thereby suppressing ionization of other sample components. Further insight as to the origin/identity of

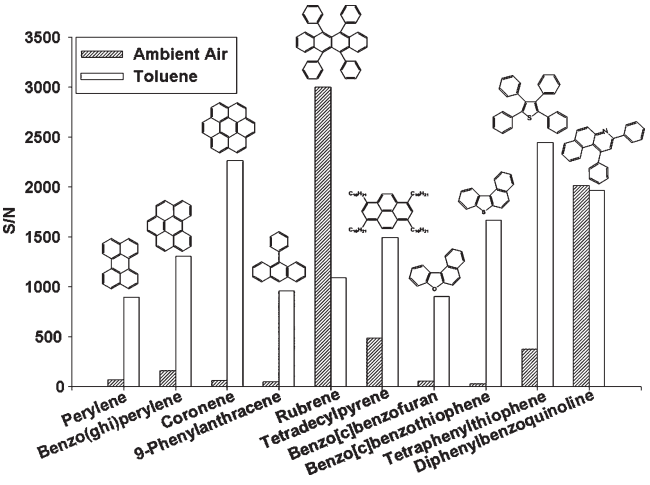

Figure 5. Signal-to-noise ratio obtained by AP/LIAD-CI for each of several petroleum model compounds for a corona discharge initiated in ambient air or in the presence of vaporized toluene.

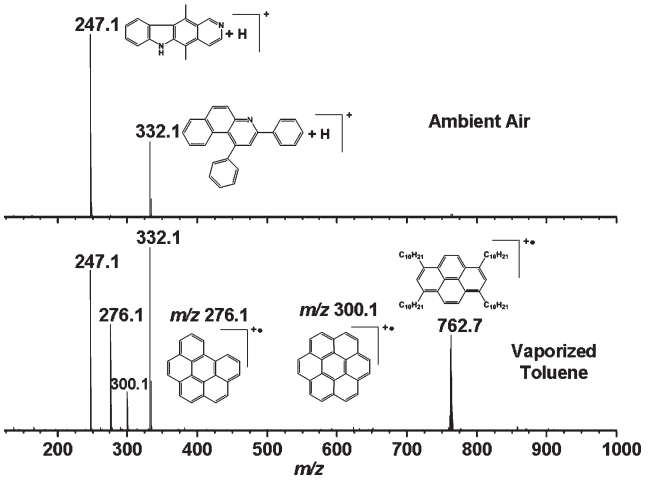

Figure 6. AP/LIAD-CI FT-ICR mass spectra for an equimolar mixture (4 μL of 0.2 mM each) of five petroleum model compounds: benzo(ghi)perylene, coronene, ellipticine, diphenylbenzoquinoline, and tetradecylpyrene, for corona discharges initiated in ambient air vs vaporized toluene.

reagent ions that effect analyte protonation is provided by doping the air surrounding the corona needle with D_2O, leading to abundant $[M + D]^+$ ions for both ellipticine and diphenylbenzoquinoline (Supporting Information Table S2). $H^+(H_2O)_n$ generated from the moisture content of the air evidently constitutes the major source of protons in the ambient air discharge.

In the presence of toluene dopant, all 5 analytes were detected (Figure 6, bottom). The nitrogen-containing analytes gave mainly $[M + H]^+$, whereas the PAHs were detected as $M^{+\bullet}$. Charge exchange reactions with toluene radical cations could account for the formation of PAH $M^{+\bullet}$; however, the origin of the protonated analytes is uncertain. We therefore performed the same experiment with toluene spiked with 5% D_2O and toluene-d_8 as dopant. All five analytes were detected for toluene with or without D_2O: the nitrogen-containing compounds were detected as $[M + H]^+$ and $[M + D]^+$, and the PAHs as $M^{+\bullet}$. However, the spiking of D_2O into toluene gave more abundant $[M + D]^+$ than when toluene-d_8 was used as dopant

dx.doi.org/10.1021/ac102543s |*Anal. Chem.* 2011, 83, 1616–1623

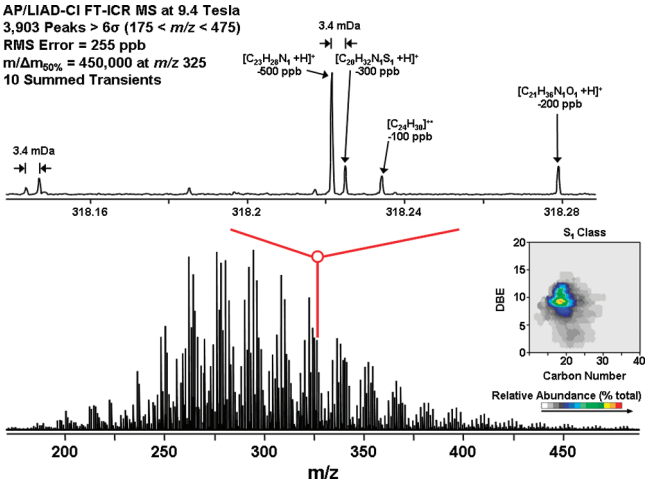

Figure 7. Broadband positive-ion AP/LIAD-CI FT-ICR mass spectrum of an Athabasca bitumen heavy vacuum gas oil (HVGO) distillation cut (400−425 °C). The mass scale-expanded inset (top) highlights the requirement for ultrahigh resolution for the analysis of petroleum samples to separate isobaric species that differ in exact mass but have the same nominal mass (e.g., species differing in elemental composition by C_3 vs SH_4, both with nominal mass of 36 Da, but differ by 3.4 mDa in exact mass). The isoabundance-contoured plot of the double bond equivalents (DBE) versus carbon number of the S_1 class is also shown.

(Supporting Information Table S2). Evidently protonated water clusters generated from the moisture content of the air could also potentially be a major source of protons for CI performed in the presence of toluene as dopant.

In summary, performing the experiment in an ambient air discharge under conditions that prohibit the formation of oxidation products can be advantageous for selective detection of the more polar nitrogen-containing sample components. Conversely, addition of toluene dopant provides a more representative fingerprint of the sample composition.

Petroleum Distillates. Figure 7 shows a broadband AP/LIAD-CI FT-ICR mass spectrum of a 400−425 °C distillation cut of an Athabasca bitumen HVGO in the presence of toluene dopant. Ten digitized time-domain ICR transients were collected for a predetermined signal magnitude threshold and averaged. The Predator data station supports conditional data acquisition, whereby acquired data is evaluated in real time and user-defined conditions must be met before the data is stored.[41] The spectrum exhibits more than 3,900 peaks (each with a magnitude higher than at least 6σ of baseline noise) between 175 < m/z < 475, at a mass resolving power ($m/\Delta m_{50\%}$, in which $\Delta m_{50\%}$ denotes the full mass spectral peak width at half-maximum peak height) of 450 000 at m/z = 325 and subparts per million mass accuracy (255 ppb rms error). The ultrahigh mass accuracy enables the resolution of isobaric species differing in elemental composition by C_3 versus SH_4, which both have a nominal mass of 36 Da (but differ by 3.4 mDa in exact mass, Figure 7, top) and defines the minimum required mass resolving power for the unambiguous assignment of elemental formulas for the thousands of peaks in the spectrum.[25−27,42,43] The inset in Figure 7 shows an example of the isoabundance-contoured plots of DBE vs carbon number for the S_1 class, in very good agreement with previously reported electrospray, atmospheric pressure photoionization, and field desorption ionization FT-ICR MS analysis of the same distillate.[26,27]

CONCLUSIONS

In summary, we present a novel laser-based matrix-free atmospheric pressure ionization technique: atmospheric pressure laser-induced acoustic desorption chemical ionization (AP/LIAD-CI). The technique decouples analyte desorption from subsequent chemical ionization by reagent ions generated by a corona discharge in ambient air or in the presence of vaporized toluene as dopant. Initial results indicate that most of the internal energy imparted during analysis is incorporated during ionization, not desorption as in vacuum/LIAD-CI. Ionization may thus be tuned according to the choice of reagent ions.[11] CI with ambient air (the most cost-effective option) achieves selective ionization of polar nitrogen-containing components in complex mixtures. However, the use of toluene dopant enables ionization of both polar and nonpolar components to give a more representative compositional fingerprint of the sample.

The coupling of the technique to FT-ICR MS takes advantage of the unmatched high mass resolution/accuracy afforded by FT-ICR as the best platform for the reliable determination of the elemental compositions of the components of complex organic mixtures. In the present configuration (up to 10 time-domain acquisitions) for the analysis of crude oil distillates already provides mass resolving power, $m/\Delta m_{50\%}$ = 450 000 at m/z 325. We are proceeding to incorporate automated sample positioning devices into the source to allow longer sampling and analysis periods, so as to provide significantly higher resolution.

ASSOCIATED CONTENT

Supporting Information. Additional material as described in the text. This material is available free of charge via the Internet at http://pubs.acs.org.

AUTHOR INFORMATION

Corresponding Author

*Tel: +1 850 644 0529 (A.G.M.); +1 850 644 1366 (R.P.R.). Fax: +1 850 644 1366. E-mail: marshall@magnet.fsu.edu (A.G.M.); rodgers@magnet.fsu.edu (R.P.R.).

ACKNOWLEDGMENT

This work was supported by NSF Division of Materials Research through DMR-06-54118, the State of Florida, and Shell Global Solutions, Houston TX. We thank Prof. Murray Gray of the University of Alberta for providing tetradecylpyrene, tetraphenylthiophene and MG 613. We thank Dr. Vladislav Lobodin for insightful discussions; John Quinn and Daniel McItosh for assistance with the design and fabrication of the LIAD probe, and Dr. Parviz Rahimi of the National Centre for Upgrading Technology for providing HVGO distillate samples.

REFERENCES

(1) Fenn, J. B.; Mann, M.; Meng, C. K.; Wong, S. F.; Whitehouse, C. M. *Science* **1989**, *246*, 64–71.

(2) Tanaka, K.; Waki, H.; Akita, S.; Yoshida, Y.; Yoshida, T. *Rapid Commun. Mass Spectrom.* **1988**, *2*, 151–153.

(3) Hillenkamp, F.; Karas, M.; Beavis, R. C.; Chait, B. T. *Anal. Chem.* **1991**, *63*, A1193–A1202.

(4) Karas, M.; Hillenkamp, F. *Anal. Chem.* **1988**, *60*, 2299–2301.

(5) Li, X. H.; Wu, X.; Kim, J. M.; Kim, S. S.; Jin, M.; Li, D. H. *J. Am. Soc. Mass Spectrom.* **2009**, *20*, 2167–2173.

(6) Wen, X. J.; Dagan, S.; Wysocki, V. H. *Anal. Chem.* **2007**, *79*, 434–444.
(7) Crawford, K. E.; Campbell, J. L.; Fiddler, M. N.; Duan, P.; Qian, K.; Gorbaty, M. L.; Kenttamaa, H. I. *Anal. Chem.* **2005**, *77*, 7916–7923.
(8) Duan, P.; Qian, K.; Habicht, S. C.; Pinkston, D. S.; Fu, M. K.; Kenttamaa, H. I. *Anal. Chem.* **2008**, *80*, 1847–1853.
(9) Golovlev, V. V.; Allman, S. L.; Garrett, W. R.; Chen, C. H. *Appl. Phys. Lett.* **1997**, *71*, 852–854.
(10) Habicht, S. C.; Amundson, L. M.; Duan, P. G.; Vinueza, N. R.; Kenttamaa, H. I. *Anal. Chem.* **2010**, *82*, 608–614.
(11) Perez, J.; Ramirez-Arizmendi, L. E.; Petzold, C. J.; Guler, L. P.; Nelson, E. D.; Kenttamaa, H. I. *Int. J. Mass Spectrom.* **2000**, *198*, 173–188.
(12) Pinkston, D. S.; Duan, P.; Gallardo, V. A.; Habicht, S. C.; Tan, X. L.; Qian, K. N.; Gray, M.; Mullen, K.; Kenttamaa, H. I. *Energy Fuels* **2009**, *23*, 5564–5570.
(13) Shea, R. C.; Habicht, S. C.; Vaughn, W. E.; Kenttamaa, H. I. *Anal. Chem.* **2007**, *79*, 2688–2694.
(14) Shea, R. C.; Petzold, C. J.; Campbell, J. L.; Li, S.; Aaserud, D. J.; Kenttamaa, H. I. *Anal. Chem.* **2006**, *78*, 6133–6139.
(15) Shea, R. C.; Petzold, C. J.; Liu, J. A.; Kenttamaa, H. I. *Anal. Chem.* **2007**, *79*, 1825–1832.
(16) Zinovev, A. V.; Veryovkin, I. V.; Moore, J. F.; Pellin, M. J. *Anal. Chem.* **2007**, *79*, 8232–8241.
(17) Lindner, B.; Seydel, U. *Anal. Chem.* **1985**, *57*, 895–899.
(18) Cheng, S. C.; Cheng, T. L.; Chang, H. C.; Shiea, J. *Anal. Chem.* **2009**, *81*, 868–874.
(19) Song, L. G.; Dykstra, A. B.; Yao, H. F.; Bartmess, J. E. *J. Am. Soc. Mass Spectrom.* **2009**, *20*, 42–50.
(20) Song, L. G.; Gibson, S. C.; Bhandari, D.; Cook, K. D.; Bartmess, J. E. *Anal. Chem.* **2009**, *81*, 10080–10088.
(21) McEwen, C. N.; Larsen, B. S. *J. Am. Soc. Mass Spectrom.* **2009**, *20*, 1518–1521.
(22) Herrera, L. C.; Grossert, J. S.; Ramaley, L. *J. Am. Soc. Mass Spectrom.* **2008**, *19*, 1926–1941.
(23) Cheng, S. C.; Huang, M. Z.; Shiea, J. *Anal. Chem.* **2009**, *81*, 9274–9281.
(24) Tan, X.; Fenniri, H.; Gray, M. R. *Energy Fuels* **2008**, *22*, 715–720.
(25) McKenna, A. M.; Blakney, G. T.; Xian, F.; Glaser, P. B.; Rodgers, R. P.; Marshall, A. G. *Energy Fuels* **2010**, *24*, 2939–2946.
(26) McKenna, A. M.; Purcell, J. M.; Rodgers, R. P.; Marshall, A. G. *Energy Fuels* **2010**, *24*, 2929–2938.
(27) Smith, D. F.; Rahimi, P.; Teclemariam, A.; Rodgers, R. P.; Marshall, A. G. *Energy Fuels* **2008**, *22*, 3118–3125.
(28) Senko, M. W.; Canterbury, J. D.; Guan, S. H.; Marshall, A. G. *Rapid Commun. Mass Spectrom.* **1996**, *10*, 1839–1844.
(29) Senko, M. W.; Hendrickson, C. L.; PasaTolic, L.; Marto, J. A.; White, F. M.; Guan, S. H.; Marshall, A. G. *Rapid Commun. Mass Spectrom.* **1996**, *10*, 1824–1828.
(30) Blakney, G. T.; Robinson, D. E.; Ly, N. V.; Kelleher, N. L.; Hendrickson, C. L.; Marshall, A. G. Presented at the 53rd American Society of Mass Spectrometry Annual Conference on Mass Spectrometery & Allied Topics, 2005, San Antonio, TX, 4−9 June, Poster TP220.
(31) Hakansson, K.; Chalmers, M. J.; Quinn, J. P.; McFarland, M. A.; Hendrickson, C. L.; Marshall, A. G. *Anal. Chem.* **2003**, *75*, 3256–3262.
(32) Beu, S. C.; Laude, D. A. *Int. J. Mass Spectrom. Ion Processes* **1992**, *112*, 215–230.
(33) Marshall, A. G.; Verdun, F. R. *Fourier Transform in NMR, Optical and Mass Spectrometry: A User's Handbook*; Elsevier: Amsterdam, the Netherlands, 1990.
(34) Freitas, M. A.; Hendrickson, C. L.; Marshall, A. G. *Rapid Commun. Mass Spectrom.* **1999**, *13*, 1639–1642.
(35) Schafer, M.; Schmuck, C.; Heil, M.; Cooper, H. J.; Hendrickson, C. L.; Chalmers, M. J.; Marshall, A. G. *J. Am. Soc. Mass Spectrom.* **2003**, *14*, 1282–1289.
(36) Kendrick, E. *Anal. Chem.* **1963**, *35*, 2146–2154.
(37) Hughey, C. A.; Hendrickson, C. L.; Rodgers, R. P.; Marshall, A. G.; Qian, K. N. *Anal. Chem.* **2001**, *73*, 4676–4681.
(38) McLafferty, F. W.; Turecek, F. *Interpretation of Mass Spectra*, 4th ed.; University Science Books: Mill Valley, CA, 1993.
(39) Cody, R. B. *Anal. Chem.* **2009**, *81*, 1101–1107.
(40) http://webbook.nist.gov/chemistry/.
(41) Blakney, G. T.; Hendrickson, C. L.; Marshall, A. G. *Int. J. Mass Spectrom.* **2011**in Press.
(42) Rodgers, R. P.; Schaub, T. M.; Marshall, A. G. *Anal. Chem.* **2005**, *77*, 20a–27a.
(43) Smith, D. F.; Schaub, T. M.; Kim, S.; Rodgers, R. P.; Rahimi, P.; Teclemariam, A.; Marshall, A. G. *Energy Fuels* **2008**, *22*, 2372–2378.